

45. H. deThe *et al.*, *ibid.* **330**, 667 (1987).
 46. W. Segaves, thesis, Stanford University (1988).
 47. M. S. Johnson and R. F. Doolittle, *J. Mol. Evol.* **23**, 267 (1986).
 48. S. Hollenberg *et al.*, *Cell* **49**, 39 (1987).
 49. P. J. Godowski *et al.*, *Nature (London)* **325**, 365 (1987).
 50. P. B. Becker *et al.*, *ibid.* **324**, 606 (1986).
 51. T. Wellman and M. Beato, *ibid.*, p. 688.
 52. V. Giguere *et al.*, *Cell* **46**, 645 (1986).
 53. V. Kumar, S. Green, A. Staub, P. Chambon, *EMBO J.* **5**, 2231 (1986).
 54. S. Green and P. Chambon, *Nature (London)* **325**, 75 (1987).
 55. J. Miller, A. McLachlan, A. Klug, *EMBO J.* **4**, 1609 (1985).
 56. R. M. Evans and S. Hollenberg, *Cell* **52**, 1 (1988).
 57. S. Hollenberg, V. Giguere, R. M. Evans, unpublished observations.
 58. M. Sabbah *et al.*, *J. Biol. Chem.* **262**, 8631 (1987).
 59. C. Huckaby *et al.*, *Proc. Natl. Acad. Sci. U.S.A.* **84**, 8380 (1987).
 60. M. Danielson *et al.*, *Mol. Endocrinol.* **1**, 816 (1987).
 61. K. Yamamoto *et al.*, *Rec. Prog. Hormone Res.* **32**, 3 (1976).
 62. V. Kumar *et al.*, *Cell* **51**, 941 (1987).
 63. B. O'Malley, personal communication.
 64. M. S. Brown and J. L. Goldstein, in *The Pharmacological Basis of Therapeutics*, A. G. Gilman, L. S. Goodman, T. W. Rall, F. Murad, Eds. (Macmillan, New York, 1985), pp. 827–845.
 65. J. Sudhof, D. Aussel, M. Brown, J. Goldstein, *Cell* **48**, 1061 (1987).
 66. A. Poland, E. Glover, A. Kende, *J. Biol. Chem.* **251**, 4936 (1976).
 67. G. W. Sledge and W. L. McGuire, *Adv. Cancer Res.* **38**, 61 (1983).
 68. T. Addison, *On the Constitutional and Local Effects of Disease of the Suprarenal Capsules* (S. Highley, London, 1855).
 69. R. M. Sapolsky, *J. Neurosci.* **6**, 2240 (1986).
 70. C. Thaller and G. Eichele, *Nature (London)* **327**, 625 (1987).
 71. S. Strickland and V. Mahdavi, *Cell* **15**, 393 (1978); A. Jetten *et al.*, *Exp. Cell. Res.* **124**, 381 (1979); S.-Y. Wang *et al.*, *Dev. Biol.* **107**, 75 (1985).
 72. M. Ptashne, *A Genetic Switch* (Cell Press, Cambridge, MA, 1986).
 73. L. Keegan, G. Gill, M. Ptashne, *Science* **231**, 699 (1986); R. Brent and M. Ptashne, *Cell* **43**, 729 (1985).
 74. I. Hope and K. Struhl, *Cell* **46**, 885 (1986).
 75. E. Giniger and M. Ptashne, *Nature (London)* **330**, 670 (1987).
 76. T. H. Morgan, in *Nobel Lectures in Molecular Biology*, D. Baltimore, Ed. (Academic Press, New York, 1977), pp. 3–18; T. H. Morgan, *The Theory of the Gene* (Yale Univ. Press, New Haven, 1926).
 77. R. Miesfeld *et al.*, *Cell* **46**, 389 (1986).
 78. M. Danielson *et al.*, *EMBO J.* **5**, 2513 (1986).
 79. M. L. Law *et al.*, *Proc. Natl. Acad. Sci. U.S.A.* **84**, 2877 (1987).
 80. C. Thompson and R. M. Evans, unpublished observations.
 81. A. Cato *et al.*, *EMBO J.* **5**, 2237 (1986).
 82. S. Rusconi *et al.*, *ibid.* **6**, 1309 (1987).
 83. M. Mattei *et al.*, *Hum. Genet.*, in press.
 84. I thank J. Arriza for helping to compile data, members of the Gene Expression Laboratory for discussion, and R. Doolittle for computer analysis of receptor homologies. I also thank G. Wahl, M. McKeown, B. Sefton, T. Hunter, and other members at the Salk Institute for advice and critical reading of the manuscript. I acknowledge many colleagues who shared data prior to publication and thank E. Stevens for expert administrative and secretarial assistance. Supported by the Howard Hughes Medical Institute and a grant from the National Institutes of Health.

Global Sea Level and Earth Rotation

W. R. PELTIER

Recent analyses of long time scale secular variations of sea level, based on tide gauge observations, have established that sea level is apparently rising at a globally averaged rate somewhat in excess of 1 millimeter per year. It has been suggested that the nonsteric component of this secular rate might be explicable in terms of ongoing mass loss from the small ice sheets and glaciers of the world. Satellite laser ranging and very long baseline interferome-

try data may be used to deliver strong constraints on this important scenario because of the information that these systems provide on variations of the length of day and of the position of the rotation pole with respect to the earth's surface geography. These data demonstrate that the hypothesis of mass loss is plausible if the Barents Sea was covered by a substantial ice sheet at the last maximum of the current ice age 18,000 years ago.

DURING THE PAST 100 YEARS, GLOBAL SEA LEVEL HAS apparently risen by 10 to 15 cm, roughly 50% of which is attributed to the thermal expansion of the oceans (1–3). As recently discussed by Meier (4), the remainder, although usually attributed to ongoing melting of the Antarctic and Greenland ice sheets, is more satisfactorily understood as a product of the present-day retreat of the small ice sheets and glaciers of the world. The reason for this is that the best available information on the contemporary mass balances of the large polar ice sheets suggests that they are near equilibrium, whereas most of the smaller systems are known to be in active retreat. If Meier's hypothesis is correct, it has important implications with respect to climate change since one might attribute the ongoing melting of the small ice sheets and

glaciers to the climate warming expected on the basis of the increase in atmospheric concentrations of CO₂ and other "greenhouse" gases that has been taking place since the beginning of the industrial revolution as a result of the burning of fossil fuels.

Relative Sea Level and Glacial Isostasy

Although the tide gauge data that have been employed to infer the existence of the above-noted secular rate of sea level rise are often strongly contaminated by geological processes, certain regions are sufficiently immune from such processes that the tide gauge records from them are especially valuable as measures of the eustatic variation. These records are probably more meaningful as measures of this variation than the direct global average of the secular rates that has usually been calculated (3). Passive continental margins

The author is professor of physics in the Department of Physics of the University of Toronto, Toronto, Ontario, Canada M5S 1A7.

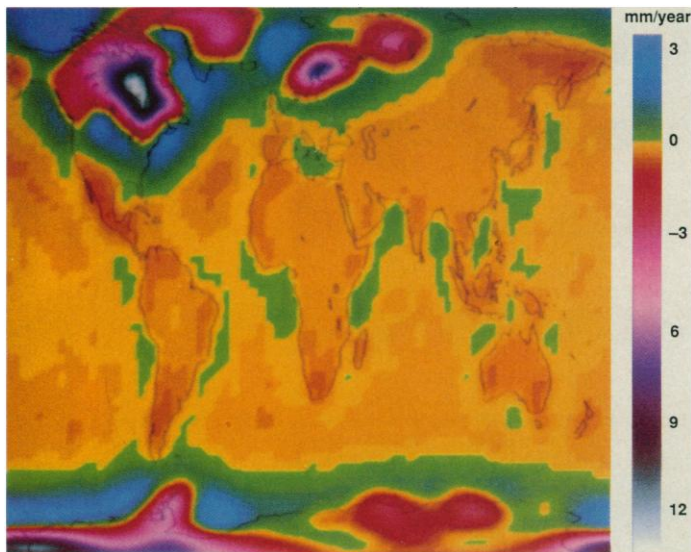


Fig. 1. Theoretical prediction of the present-day rate of change of geoid height with respect to the surface of the solid earth owing to the influence of the disintegration of the continental ice sheets that existed at the last glacial maximum 18,000 years ago. Over the oceans the geoid is coincident with the ocean surface and the map therefore represents the rate of sea level change resulting from deglaciation, which should be measured today by a tide gauge attached to the solid earth.

such as those of the east coasts of North and South America are examples of such regions. Unfortunately, the most heavily instrumented of these coastlines, that of eastern North America, is still substantially affected by relative sea level variations caused by the retreat of the vast Laurentide ice sheet, which last covered all of Canada and the northeastern United States at ice age maximum 18,000 years ago. Fortunately, however, a rather accurate model is available (5) that may be employed to filter the signal that is due to glacial isostatic adjustment from the tide gauge data. Figure 1 shows the predicted rate of relative sea level change (in millimeters per year) that should be occurring everywhere on the earth's surface as a consequence of this last deglaciation event of the present ice age. Inspection of this figure demonstrates that the global map of the present-day rate of relative sea level change is dominated by the rapid ongoing fall of sea level in each of the three regions that were previously ice covered (Laurentia, Fennoscandia, and Antarctica). In these regions the rates of sea level fall are approximately 1 cm year^{-1} . Surrounding them are ring-shaped regions in which relative sea level is predicted to be rising at rates in excess of 1 mm year^{-1} . In the far field of the ice sheets a slow rise of sea level is predicted for most continental coastlines and a slow fall of sea level at oceanic island locations. This theoretical model may be employed to filter from modern tide gauge measurements of the secular sea level change the contribution that is the result of glacial isostatic disequilibrium.

Figure 2 illustrates the results that have been obtained by application of this technique to analyze observed tide gauge secular sea level trends from all of the gauges located along both the U.S. east coast (passive margin) and the U.S. west coast (active margin). The raw data employed are those from the recently published *National Ocean Service Catalog* (6), and on the figure the filtered data are shown as solid crosses that are plotted as a function of distance in degrees of arc from the southernmost gauge along the coast. On the U.S. east coast the southernmost gauge is at Key West, Florida, and on the west coast it is at San Diego (7). The correction actually applied to the raw data is shown as the thin solid line, which is bracketed by dashed and dotted lines intended to denote the magnitude of the error that could be associated with the correction.

The mean of the residual rates of sea level rise for the U.S. east coast is about 1.3 mm year^{-1} , in accord with previous estimates of the present-day eustatic rate cited above. For the U.S. west coast active margin, the scatter is clearly so large that the average would not be meaningful and it has therefore not been shown. Although the scatter about the mean of the residual data from U.S. east coast sites is considerable, implying that processes other than a smooth eustatic sea level rise are contributing to the observed variability, the systematic positive bias of the residual for all but one of the 26 east coast tide gauges is rather compelling evidence that a eustatic sea level rise is presently occurring.

The fraction of this eustatic rise that is attributable to the steric effect of thermal expansion of the oceans is not well known, but the best available estimates (2, 8) suggest that only 50 to 60% of the signal is explicable in these terms, leaving an unexplained contribution of approximately 0.5 mm year^{-1} , which requires for its explanation an actual increase of the mass of water in the global ocean. It is the source of this contribution that Meier's hypothesis addresses. To appreciate the magnitude of the effect that this number represents it might usefully be compared to the rate of eustatic sea level rise that was produced by the last deglaciation event of the current ice age. Beginning approximately 18,000 years ago and ending about 6,000 years ago the complete disintegration of the Laurentian and Fennoscandian ice complexes, along with much of the West Antarctic ice sheet, led to the addition of water to the global ocean, which raised sea level by approximately 120 m. Even during the glacial-interglacial transition itself the average rate of eustatic sea level rise was therefore only 10 mm year^{-1} , barely one order of magnitude in excess of the eustatic rate inferred from contemporary tide gauge data.

The Rotational Response to Ice Sheet Accretion and Disintegration

Given the large redistribution of mass on the earth's surface that is implied by a nonsteric eustatic rise of 0.5 mm year^{-1} it should not be particularly surprising that substantial dynamical effects on the planet would thereby be produced. Foremost among these are the effects on the earth's state of rotation that will be caused by variations of the moment of inertia tensor of the planet that are associated with the redistribution of surface mass. In order to employ rotation observations to investigate the plausibility of Meier's hypothesis, however, we are obliged to filter from them the ongoing effects associated with the last deglaciation event of the current ice age. The rotational data, as we will show, are as "contaminated" by the influence of this dynamical event as are the tide gauge-measured rates of relative sea level change discussed in connection with Fig. 1. Only if we can accurately remove this contamination will it be possible to employ the rotational observables to quantitatively assess the plausibility of Meier's hypothesis of contemporary ice sheet melting.

A dynamical theory has also been developed that may be used to accurately predict the rotational effects that should be observed today as residual signatures of the last deglaciation event (5, 9). In fact this theoretical model has been used to demonstrate that the two principal signatures of the earth's rotational state that should be influenced by this event have values that make them entirely explicable in terms of this single cause. These two signatures are, respectively, the so-called "nontidal" component of the acceleration of the earth's axial rate of rotation, and the true drift of the rotation pole with respect to the surface geography. Although the former effect was originally inferred on the basis of ancient eclipse data (10), it has recently been reconfirmed in rather convincing fashion

through reduction of laser ranging data for the LAGEOS satellite (11). The observation of the true drift of the pole has a history that has been similarly affected by the application of modern space-based geodetic techniques. This polar wander signal was originally inferred by means of data from the network of photo-zenith tube observatories of the International Latitude Service (ILS) (12) and has been reconfirmed in a preliminary fashion by application of recent very long baseline interferometry (VLBI) observations (13). Because both of these rotational observables have been shown to be entirely explicable as effects arising from the last deglaciation event of the current ice age (5, 9), we might naturally be interested whether the observations would allow for the action on the planet of the additional rotational forcing that is represented by the eustatic sea level variation required by Meier's hypothesis. As I shall demonstrate, Meier's hypothesis is tenable with respect to the rotational constraints if a rather substantial ice sheet existed in the vicinity of the Barents Sea during the last glacial maximum. The existence of the Barents Sea ice sheet has often been suggested in the past but no convincing argument, other than the original one based upon ^{14}C -controlled relative sea level histories from islands in this region (14), has been presented.

The theoretical predictions of both of the above-described components of the planet's rotational response to surface loading by ice sheets have forms that have been previously presented in the literature (5, 9). For the nontidal acceleration the prediction is:

$$\frac{\dot{\omega}_3}{\Omega} = -\frac{I_{33}^R}{C} \left[D_1 \dot{f}(t) + \sum_{j=1}^M r_j \frac{d}{dt} [f(t) \exp(-s_j t)] \right] \quad (1)$$

where

$$I_{33}^R = \sum_{i=1}^N M_i a_i^2 \left[\frac{2}{15} \frac{a_{20}}{a_{00}} - \frac{1}{3} \cos \alpha_i (1 + \cos \alpha_i) P_2^0(\cos \theta_i') \right] \quad (2)$$

is the change of the axial component of the moment of inertia tensor that would be produced by N circular cap ice sheets of radius α_i ($i = 1, \dots, N$) and mass M_i ($i = 1, \dots, N$) with centers at latitude θ_i' and longitude ϕ_i' . The N ice sheets are assumed to discharge their meltwater to, and accrete water from, geographically realistic oceans described by the ocean function (15), which determines the values of the spherical harmonic coefficients a_{20} and a_{00} . Also in Eq. 1, C is the axial moment of inertia of the unperturbed oblate earth; $D_1 = 1 + k_2^{LE}$, in which k_2^{LE} is the elastic surface load Love number of degree 2; and $f(t)$ is the history function of ice sheet loading and unloading, which is assumed to be common to all of the Quaternary ice sheets that have been collectively involved in the 10^5 -year periodic cycle of glaciation and deglaciation that has characterized the Quaternary period of earth history. For the purpose of all of the calculations to be reported here I will approximate the histories of the Quaternary ice sheets by five identical 10^5 -year cycles of sawtooth form, each consisting of a 9×10^4 -year linear glaciation phase and a 10^4 -year linear deglaciation phase that satisfy the constraints imposed by $\delta^{18}\text{O}$ data from deep sea sedimentary cores (16). The remaining parameters in Eq. 1, r_j and s_j , are the amplitudes and inverse decay times of the M normal modes of viscous gravitational relaxation that are required to synthesize the degree 2 component of the response of the viscoelastic planet to surface load forcing [see (5), for example]. In order to integrate the additional 31 glaciers and ice sheets that are presently active according to Meier's hypothesis into the solution, they are simply added together with the three (or four) main Quaternary ice masses with appropriate individual history functions, which are taken to consist of simple linear local deglaciation histories of strength determined according to table 1 of Meier (4) and which are assumed to have been active

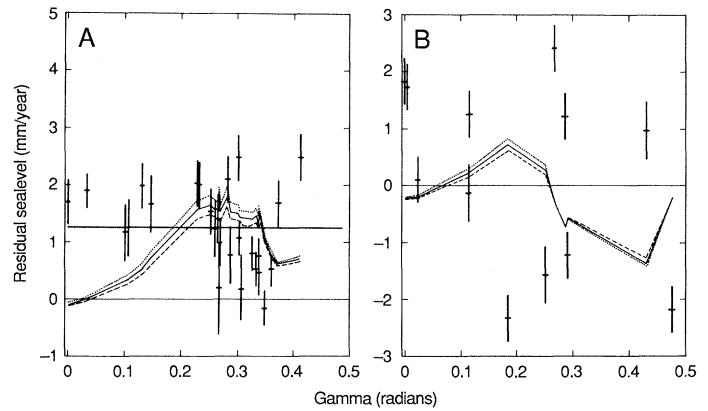


Fig. 2. Tide gauge rates of secular sea level change corrected for the effect of present-day glacial isostatic adjustment shown in Fig. 1. The residual rates are shown for both the U.S. east coast (A) and the U.S. west coast (B). The corrections derived from the global theoretical calculation (with model CML64G) illustrated in Fig. 1 are shown as the thin solid (average rate, 17,000 to 19,000 years) line, which is bracketed by dashed (average rate, 18,000 to 19,000 years) and dotted (average rate, 17,000 to 18,000 years) lines intended to represent the possible error in the computed correction. Note that for the U.S. east coast passive margin data, although the scatter about the mean residual rate of rise is considerable, there is a marked systematic departure from zero. It is the nonsteric part of this systematic departure that Meier's hypothesis purports to explain. The data from the tectonically active west coast margin provide no useful constraint on this scenario.

over the last 10^2 years, essentially since rapid industrialization began.

For the polar wander response to glacial loading and unloading the solution (5, 9) has the somewhat more complex form:

$$\begin{bmatrix} \dot{\omega}_1 \\ \dot{\omega}_2 \\ \dot{\omega}_3 \end{bmatrix} = \frac{\Omega}{A \sigma_0} [I_{13}^R, I_{23}^R] \cdot \left[D_1 \dot{f}(t) + D_2 f(t) + \sum_{i=1}^{M-1} E_i \frac{d}{dt} [f(t) \exp(-\lambda_i t)] \right] \quad (3)$$

in which Ω is the unperturbed initial axial rate of rotation, A is the equatorial moment of inertia, σ_0 is the Chandler wobble frequency, and I_{13}^R and I_{23}^R are the perturbations of the off-diagonal elements of the inertia tensor, which would be produced by the shifting surface load if the earth were rigid. These latter have the forms (9)

$$I_{13}^R = \sum_{i=1}^N M_i a_i^2 \left[\frac{1}{6} \cos \alpha_i (1 + \cos \alpha_i) P_2^1(\cos \theta_i') \cos \phi_i' - \frac{a_{21}}{5a_{00}} \right] \quad (4)$$

$$I_{23}^R = \sum_{i=1}^N M_i a_i^2 \left[\frac{1}{6} \cos \alpha_i (1 + \cos \alpha_i) P_2^1(\cos \theta_i') \sin \phi_i' - \frac{b_{21}}{5a_{00}} \right] \quad (5)$$

which are similar to the expression for I_{33}^R and involve spherical harmonic amplitudes, a_{21} and b_{21} , in the expansion of the ocean function (15). The remaining parameters in Eq. 3 (D_2 , E_i , and λ_i) are complicated functions of the radial viscoelastic structure and are defined in the previously cited papers (5, 9). I shall use the above theoretical results to investigate the constraints that observations of the nontidal acceleration and true polar wander place upon Meier's hypothesis of the origin of the secular sea level rise that appears to be required to understand tide gauge observations.

Rotational Constraints on Meier's Hypothesis

I have used table 1 of Meier (4) to compute the elements of the rotational forcing function (I_{33}^R , I_{13}^R , and I_{23}^R) that are contributed by

the small ice sheets and glaciers to the solutions represented by Eqs. 1 and 3. The locations of these ice sheets and glaciers, and the relative strengths of their contributions to the eustatic rise according to Meier's hypothesis, are shown in Fig. 3. These are tabulated in Table 1 for two cases denoted by I and II. In the first case, each of the I_{ij}^R is computed on the basis of an assumed mass loss per year of $0.23aG$ where a and G in Meier's analysis are, respectively, the annual mass balance amplitude and the glacier area, with aG being the amplitude area product (in km^3/year), which he has tabulated separately. For case II this number has been replaced by the product $\bar{b}G$ where \bar{b} are long-term balances wherever these are known. Since the case II results are the most accurate according to Meier's analysis, I shall use them for all of the final analyses although the two cases will be compared at intermediate stages. Because the rotational data are as contaminated by the influence of the last deglaciation event as are the tide gauge observations themselves, I am obliged to include these influences in my analyses by means of Eqs. 1 and 3. To do so I require I_{ij}^R for the ice sheets that existed at Würm-Wisconsin maximum and have employed for this purpose the data listed in

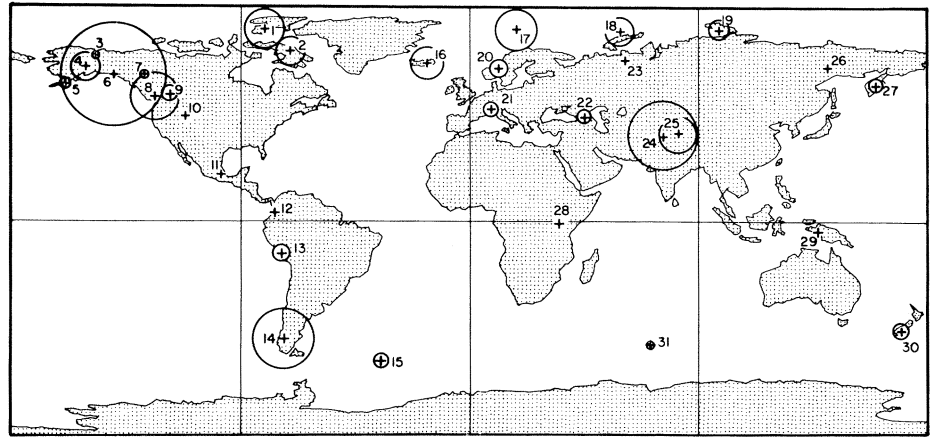
Tables 2 and 3, which, with the exception of those for the proposed Barents Sea ice sheet, are the same parameters that I have previously computed (5, 9) for these ice masses.

Figure 4 compares the influence of the extra rotational forcing, which is the result of contemporaneous melting of the small ice sheets and glaciers in Meier's hypothesis, upon the predictions of the nontidal acceleration and related \bar{J}_2 parameters to the predictions of a model that includes only the forcing due to Quaternary glaciation and deglaciation. In this figure the curve marked with the diamonds denotes the predicted nontidal acceleration for the model with no contemporary ice sheet melting, as a function of lower mantle viscosity with the upper mantle value held fixed to the value of 10^{21} Pa-sec required by relative sea level data (9) and with the lithospheric thickness equal to 120.7 km. Figure 4, a and b, compares these predictions for two different models of the radial elastic structure, CML64 and 1066B [see (9) for details], which differ from one another only in terms of the strength of the nonadiabatic stratification of density in their interiors. Superimposed upon each plate are predictions for three different versions of the calculation when the

Table 1. Geographical locations and meltwater contributions of the 31 small ice sheets and glaciers contributing to present-day eustatic water rise according to Meier's hypothesis. The perturbations of inertia caused by the annual mass loss are given for each source separately under the assumption that each source may be adequately approximated as a point mass. Numbers in first column correspond to map locations in Fig. 3.

Glacial region	Colatitude	East longitude	Case I: Mass loss per year = $0.23aG$					Case II: Mass loss per year = $\bar{b}G$ when available, else = $0.23aG$				
			Mass (10^{14} kg)	I_{13}^R (10^{28} $\frac{\text{kg}}{\text{m}^2}$)	I_{23}^R (10^{28} $\frac{\text{kg}}{\text{m}^2}$)	I_{33}^R (10^{28} $\frac{\text{kg}}{\text{m}^2}$)	Water (mm/year)	Mass (10^{14} kg)	I_{13}^R (10^{28} $\frac{\text{kg}}{\text{m}^2}$)	I_{23}^R (10^{28} $\frac{\text{kg}}{\text{m}^2}$)	I_{33}^R (10^{28} $\frac{\text{kg}}{\text{m}^2}$)	Water (mm/year)
1. Canadian Arctic-North	11.	279.	6.900	0.04	-0.57	1.84	0.019					
2. Baffin & Bylot Is., Labrador	20.	289.	3.910	0.14	-0.51	0.91	0.011					
3. Brooks Range, Kigluaik Mtns.	22.	213.	0.138	-0.02	-0.01	0.03	0.000	0.140	-0.02	-0.01	0.03	0.000
4. Alaska Range; Talkeetna, Kilbuk Mtns.	27.	209.	3.680	-0.55	-0.32	0.73	0.010	8.195	-1.23	-0.72	1.62	0.023
5. Aleutian Is., Alaska Pen.	34.	201.	0.506	-0.09	-0.04	0.08	0.001					
6. Coastal Mtns., Kenai Pen. to 55N	30.	220.	51.750	-7.28	-6.24	9.29	0.143	35.360	-4.97	-4.27	6.35	0.098
7. MacKenzie, Selwin, Rockies N of 55N	30.	232.	0.207	-0.02	-0.03	0.04	0.001					
8. Coast Mtns. S of 55N, Cascades, Olympics	39.	236.	10.350	-1.21	-1.78	1.24	0.029	9.940	-1.16	-1.71	1.19	0.028
9. Rockies S of 55N, Selkirks (CAN), N Rocky Mtns.	38.	242.	1.196	-0.12	-0.22	0.15	0.003	0.880	-0.09	-0.16	0.11	0.002
10. Middle & S Rockies, Sierra Nevada	47.	248.	0.046	0.00	-0.01	0.00	0.000	0.34	0.00	-0.01	0.00	0.000
11. Mexico	71.	262.	0.002	0.00	0.00	0.00	0.000					
12. Andes (10N to 0N)	86.	283.	0.012	0.00	0.00	0.00	0.000					
13. Andes (0S to 30S)	103.	286.	1.173	-0.04	0.09	-0.12	0.003					
14. Andes (30S to 55S)	138.	287.	17.710	-1.15	3.28	1.76	0.049					
15. S Atlantic Is.	147.	325.	0.943	-0.15	0.09	0.15	0.003					
16. Iceland, Jan Mayen	25.	343.	4.830	0.69	-0.26	1.01	0.013	7.119	1.02	-0.38	1.48	0.020
17. Svalbard	11.	18.	7.820	0.52	0.12	2.08	0.022					
18. Franz Josef Is., Novaya Zemlya	12.	59.	3.450	0.13	0.22	0.91	0.010	4.901	0.18	0.31	1.29	0.014
19. Severnaya Zemlya, other Soviet Arctic Islands	11.	98.	1.702	-0.03	0.12	0.45	0.005					
20. Norway, Sweden	27.	11.	1.541	0.24	0.04	0.30	0.004	0.651	0.10	0.02	0.13	0.002
21. Alps, Pyrenees	44.	8.	0.851	0.17	0.02	0.07	0.002	1.1218	0.24	0.03	0.10	0.003
22. Caucasus, Turkey, Iran	47.	45.	0.805	0.11	0.11	0.05	0.002	0.420	0.06	0.06	0.03	0.001
23. Ural Mtns., Byrranga, Putorana	24.	61.	0.046	0.00	0.01	0.01	0.000	0.035	0.00	0.00	0.01	0.000
24. Hindukush, Pamir, Alai, Karakorum, Himalaya, . . .	55.	76.	23.690	0.95	4.20	0.21	0.066					
25. Tien Shan, Kun Lun, Altai, Qilian Shan, . . .	54.	82.	6.210	0.13	1.14	0.10	0.017	0.642	0.01	0.12	0.01	0.002
26. Kodar, Orulgan, Chersky, Sun-Kho, Koryasky	27.	141.	0.092	-0.01	0.01	0.02	0.000					
27. Kamchatka	34.	160.	0.759	-0.14	0.04	0.12	0.002					
28. Africa	91.	35.	0.002	0.00	0.00	0.00	0.000					
29. West Irian	94.	137.	0.009	0.00	0.00	0.00	0.000					
30. New Zealand	135.	170.	1.104	0.21	-0.05	0.09	0.003					
31. Kerguelen, Heard Is.	141.	71.	0.207	-0.01	-0.04	0.02	0.001					
Totals			151.6	-7.5	-0.6	21.5	0.42	136.3	-5.6	0.0	20.0	0.38

Fig. 3. Locations of the 31 small ice sheets and glaciers that are also contributing to the present-day rate of relative sea level change according to Meier's (4) hypothesis. The relative contributions of each of these sources are represented by the radius of the circle centered on each location, and the location numbers correspond to the sites whose geographic place names are listed in Table 1.



extra forcing implied by Meier's hypothesis is included in the analysis. The triangles, squares, and circles distinguish for the prediction based on case II of Table 1 and for two variants that involve small variations of the load assumed to be emanating from the Kenai Peninsula of Alaska (a 50% reduction) and the Hindukush, respectively. As will be evident by inspection of Fig. 4, on which the observed nontidal acceleration according to Yoder *et al.* and Rubincam (11) is denoted by the two solid and two dashed lines, respectively, the addition of the forcing that results from the contemporary melting of Meier's sources simply shifts the value of the lower mantle viscosity required to fit the data to higher values. Although this shift is modest (a factor of 2 to 3) it is nevertheless completely sufficient to be excluded by the ^{14}C -controlled sea level data from sites within the ice sheet margins (7, 18). It would therefore appear that Meier's hypothesis is not compatible with the requirement of these data for an almost uniform mantle viscosity profile and therefore must be rejected.

Figure 5 shows the results of a complementary analysis of the influence of Meier's hypothesis in terms of polar wander speed and direction; this analysis also illustrates in Fig. 5, a and b, the effect of the elastic parameterization upon the outcome of the analysis. On this figure the solid curves are all model predictions of polar wander speed, whereas the dashed curves are model results for polar wander direction. The standard error bounds on the observed speed and direction according to the ILS data are shown by the horizontal solid and dashed lines, respectively. It will be observed that the incorporation of the extra forcing has essentially no effect on the predicted polar wander speed. As I have demonstrated elsewhere [(9), for example] this prediction may be made to fit the observation for the same weak viscosity contrast model that fits well the relative sea level data mentioned above simply by moderately thinning the lithosphere. However, the same is not the case for the predicted polar wander direction, which is shifted markedly to the west and well outside the bounds allowed by the ILS observations, irrespective of which version of Meier's hypothesis is employed [that is, case I (squares), case II (triangles), or an enhanced case ($0.253aG$, circles)]. It would therefore appear that Meier's hypothesis is strongly rejected by both rotational observables.

The Role of the Barents Sea Ice Sheet

We may well ask the question, however, as to what additional source of late Quaternary melting might be needed to allow for the present-day eustatic water rise that seems to be required on the basis of the tide gauge-based relative sea level analyses presented in Fig. 1. We clearly require an ice load that will enhance the predicted

nontidal acceleration so as to allow once more the reconciliation of this datum with an essentially isoviscous model of the mantle. Any sufficiently large ice sheet located near the rotation pole will clearly be adequate to accomplish this. However, in order to swing the predicted direction of polar wander back toward the east, the ice sheet must lie to the east of the eastern margin of the Atlantic Ocean. In fact there is only one location that is plausible for this ice mass and that is in the Barents Sea. The existence or nonexistence of an ice sheet covering this region has been a subject of considerable debate

Table 2. Ice sheet parameters.

Ice sheet	Mass M_i (10^{19} kg)	Radius α_i (deg)	Colatitude θ_i (deg)	East longitude ϕ_i (deg)
Laurentia	2	15	30	270
Fennoscandia	0.56	9.5	25.5	25.0
Antarctica	0.70	20.0	180.	—
Barents Sea	0.60	6.0	15.0	50.0

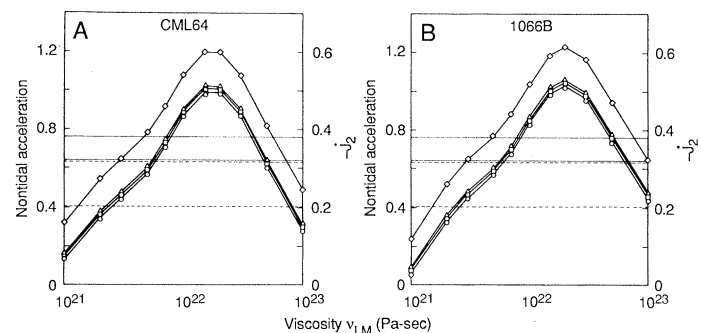


Fig. 4. Theoretical predictions of the nontidal acceleration of rotation as a function of the viscosity of the earth's mantle beneath a depth of 670 km. The upper mantle viscosity is fixed in all calculations to the value of 10^{21} Pa-sec required by ^{14}C -controlled relative sea level data observed in the time window from about 10^4 years before present until the present (5). (A) and (B) display the influence on the theoretical predictions of the radial elastic structure assumed for the earth model. The diamonds show the prediction for a scenario in which the only contributions to the present rate of nontidal acceleration are the now disappeared Pleistocene ice sheets, whereas the other curves denote predictions for the three different versions of Meier's hypothesis: triangles, contributions from the Laurentia (L), Fennoscandia (F), and Antarctica (A) ice sheets; squares, L + F + A but with Kenai = $0.5bG$ and Hindukush = $2 \times 0.23aG$; and circles, L + F + A but with Hindukush = $4 \times 0.23aG$. The horizontal solid and dashed lines illustrate the LAGEOS inferences of Yoder *et al.* and Rubincam, respectively (11). Nontidal acceleration and \dot{J}_2 are in units of 10^{-10} per year.

Table 3. Inertia perturbations I_{13}^R with realistic oceans.

Ocean	I_{13}^R (kg m ²)	I_{23}^R (kg m ²)	I_{33}^R (kg m ²)
Laurentia only	1.203×10^{31}	3.491×10^{32}	-3.420×10^{32}
Fennoscandia only	-7.504×10^{31}	-3.227×10^{31}	-1.130×10^{32}
Antarctica only	4.211×10^{30}	5.370×10^{30}	-1.799×10^{32}
Barents Sea only	-3.521×10^{31}	-4.165×10^{31}	-1.511×10^{32}

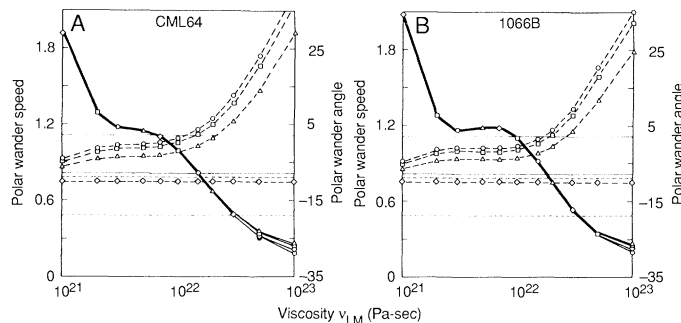


Fig. 5. Theoretical predictions of the present-day polar wander speed (in degrees per million years, solid curves) and direction (in degrees north of due west, dashed curves) for the same sequence of models (A and B) employed in Fig. 4, also as a function of the lower mantle viscosity with the upper mantle value held fixed to 10^{21} Pa-sec as required by ^{14}C -controlled relative sea level histories. Note that every version of the calculation that includes Meier's hypothesis, (L + F + A) + M, predicts a present-day direction of polar wander that does not match the direction observed in the ILS data, the standard error bounds on which are shown as the horizontal dashed lines. The solid horizontal lines show the corresponding error bounds on polar wander speed. Diamonds, L + F + A; squares, L + F + A + M, with $0.23aG$; circles, L + F + A + M with $0.253aG$; and triangles, L + F + A + M with bGM and $0.253aG$.

in the Quaternary geological community ever since its existence was first suggested by Schytt and others (14). The evidence for and against such an ice sheet covering the Barents Sea region, in which bathymetric depths are not greater than 200 m today, has been summarized recently in (18). Suffice it to say that these arguments have proven inconclusive.

In Fig. 6, I show the effect on the nontidal acceleration prediction of adding a Barents Sea ice sheet of the mass and radius listed in Table 2 to the rotational excitation function for this observable. Inspection of this figure shows that with this additional forcing the predicted nontidal acceleration is increased by precisely the amount required to reconcile the observation with the same almost isoviscous model of the mantle that is required by the relative sea level observations. Figure 7 presents a similar analysis for the predicted speed and direction of polar wander. Clearly the addition of the extra rotational forcing associated with the Barents Sea ice sheet also has precisely the effect upon the predicted direction of polar wander that is required to bring this prediction back into accord with the observed direction (under the assumption that Meier's hypothesis provides the correct explanation of the inferred nonsteric rate of secular sea level rise that is apparently required by the tide gauge observations). The mass that would have to be contained in this ice sheet in order to effect this reconciliation is rather substantial, of the same order in fact as that which was bound in the nearby land-based Fennoscandian complex.

That such a large additional source of meltwater is in fact required can also be argued from a completely different point of view. It has been understood for almost 20 years that $\delta^{18}\text{O}$ observations from deep sea sedimentary cores, when calibrated against present-day $\delta^{18}\text{O}$ from the polar ice sheets and from the global oceans, suggest that the total rise of sea level following deglaciation must have been greater than 100 m. Best present estimates (16) are in fact close to

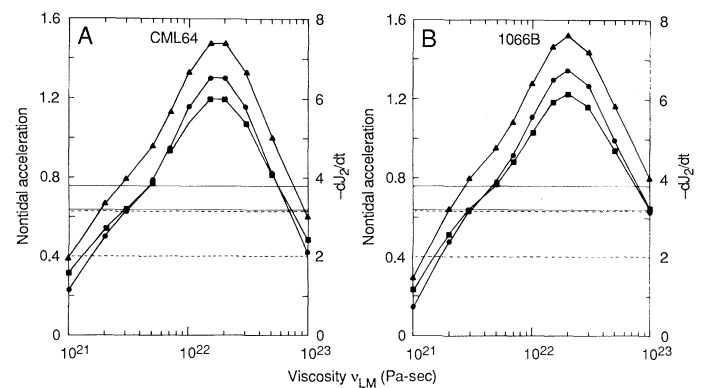


Fig. 6. Same as Fig. 4 but including the extra rotational forcing associated with a later Pleistocene Barents Sea ice sheet. Solid squares, L + F + A; solid triangles, L + F + A + B, where B stands for Barents Sea contribution; and solid circles, L + F + A + B + M, with bG or $0.23aG$.

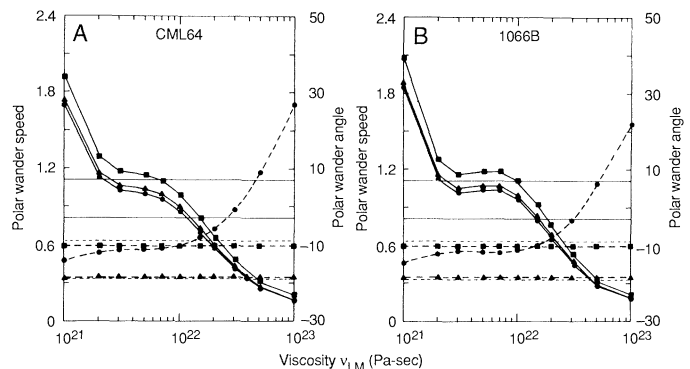


Fig. 7. Same as Fig. 5 but including the extra rotational forcing associated with a late Pleistocene Barents Sea ice sheet. Same symbols as Fig. 6.

120 m. Adding the contributions to global relative sea level rise for each of the ice sheets from the entries in the first column of Table 2 gives a total eustatic rise of 106.9 m. Although still somewhat below that suggested by $\delta^{18}\text{O}$ data, this number is within the error bounds of this inference. Without the incorporation of the Barents Sea ice sheet it is not.

Conclusions

The analysis presented in this article demonstrates very clearly, I believe, the enormous potential of extremely accurate measurements of the earth's rotation in contributing to the ongoing debate about present global sea level change. Sufficiently accurate geophysical models now exist that offer the prospect of employing modern SLR and VLBI data to discriminate between competing hypotheses. Using the best presently available data and models, I have shown that Meier's hypothesis of the origin of the tide gauge-inferred rise of global sea level is compatible with these data if one allows for the existence of a substantial Barents Sea ice sheet at the last glacial maximum. As the accuracy of modern space-based geodetic techniques improves, allowance will doubtless have to be made for further refinement of the distribution of land ice at the last glacial maximum, but the main conclusion concerning the plausibility of Meier's hypothesis is not likely to be influenced in this process. This conclusion is clearly of considerable importance in the context of the debate concerning contemporary climate change.

REFERENCES AND NOTES

1. R. Etkins and E. S. Epstein, *Science* 215, 287 (1982); R. R. Revelle, in *Changing Climate* (National Academy of Sciences, Washington, DC, 1983), pp. 443-448;

1. A. Robock, *Science* **219**, 996 (1983).
2. V. Gornitz, S. Lebedeff, J. Hansen, *Science* **215**, 1611 (1982).
3. T. P. Barnett, *Clim. Change* **5**, 15 (1983).
4. M. F. Meier, *Science* **226**, 1418 (1984).
5. W. R. Peltier, *Adv. Geophys.* **24**, 1 (1982).
6. *National Ocean Service Catalog* (National Oceanic and Atmospheric Administration, Rockville, MD, 1983).
7. W. R. Peltier, *J. Geophys. Res.* **91**, 9099 (1986).
8. D. Roemmich and C. Wunsch, *Nature (London)* **307**, 447 (1984); D. Roemmich, in *Glaciers, Ice Sheets, and Sea Level: Effect of a CO₂-Induced Climatic Change* (National Research Council, Washington, DC, 1984), pp. 104–115.
9. W. R. Peltier, *Nature (London)* **304**, 434 (1983); P. Wu and W. R. Peltier, *Geophys. J. R. Astron. Soc.* **76**, 753 (1984); W. R. Peltier, *J. Geophys. Res.* **90**, 9411 (1985).
10. P. M. Müller and F. R. Stephenson, in *Growth Rhythms and History of the Earth's Rotation* (Wiley, New York, 1975).
11. C. F. Yoder *et al.*, *Nature (London)* **303**, 757 (1983); D. P. Rubincam, *J. Geophys. Res.* **89**, 1077 (1984).
12. R. O. Vincente and S. Yumi, *Publ. Int. Latit. Obs. Mizusawa* **7**, 41 (1969); *ibid.*, p. 109.
13. W. E. Carter, D. S. Robertson, T. E. Pyle, J. Diamante, *Geophys. J. R. Astron. Soc.* **87**, 3 (1986).
14. V. Schytt, G. Hoppe, W. Blake, Jr., M. G. Grosswald, publ. no. 79, Internat. Assoc. of Scientific Hydrology, I.U.G.G., General Assembly of Bern (1967).
15. K. Lambeck, *The Earth's Variable Rotation: Geophysical Causes and Consequences* (Cambridge Univ. Press, London, 1980).
16. N. J. Shackleton and N. D. Opdyke, *Quat. Res.* **3**, 39 (1973).
17. J. Chappell and N. J. Shackleton, *Nature (London)* **324**, 137 (1986).
18. W. R. Peltier, R. A. Drummond, A. M. Tushingham, *Geophys. J. R. Astron. Soc.* **87**, 79 (1986).
19. G. H. Denton and T. J. Hughes, Eds., *The Last Great Ice Sheets* (Wiley, New York, 1981).
20. I am indebted to R. Drummond for her assistance in performing the computations discussed in this article and to A. Sousa for "processing the words."

Research Articles

Synaptic Rearrangement During Postembryonic Development in the Cricket

A. CHIBA, D. SHEPHERD,* R. K. MURPHEY†

Synaptic rearrangement during development is a characteristic of the vertebrate nervous system and was thought to distinguish vertebrates from the invertebrates. However, examination of the wind-sensitive cercal sensory system of the cricket demonstrates that some identified synaptic connections systematically decrease in strength as an animal matures, while others increase in strength over the same period. Moreover, a single sensory neuron could increase the strength of its synaptic connection with one interneuron while decreasing the strength of its connection with another interneuron. Thus, rather than being a hallmark of the vertebrate nervous system, synaptic rearrangement is probably characteristic of the development of many if not all nervous systems.

ONE IMPORTANT DISCOVERY IN NEUROBIOLOGY HAS BEEN that neural circuits are refined as an animal matures. One manifestation of this phenomenon is called "synaptic rearrangement," and can be observed in a variety of neural subsystems (1). In some situations, such as the visual cortex and the neuromuscular junction, synaptic rearrangement refines an initially diffuse set of connections (2). In others, such as the visual system of lower vertebrates, it compensates for differential patterns of growth in the retina and tectum (3). Invertebrate nervous systems, in contrast, are thought to be under a more rigid, presumably genetic, control and therefore are not likely to exhibit synaptic rearrangement or any other refinements as the animal matures (4).

The authors are at the Neurobiology Research Center, Department of Biology, State University of New York at Albany, Albany, NY 12222.

*Present address: Department of Zoology, Cambridge University, Cambridge, England.

†To whom all correspondence should be addressed.

However, a new view is emerging which suggests that the mechanisms for nervous system assembly are much the same in vertebrates and invertebrates (5). One invertebrate nervous system that is receiving considerable attention in this regard is the wind-sensitive, cercal sensory system of orthopteran insects: crickets, cockroaches, and locusts (6). This neural circuit triggers escape from approaching predators, and the first-order interneurons encode a number of features of the wind stimuli, including wind direction, velocity, and acceleration. The transducers are wind-sensitive hairs each of which is innervated by a single sensory neuron. In the adult cricket these sensory neurons synapse with the first-order interneurons in very selective ways, conferring on the interneurons particular response properties. Once established, these synaptic connections were assumed to be constant (7–9). However, examination of synaptic connections in crickets of different ages demonstrates continual changes in synaptic connections as an animal matures.

Change of synaptic strengths during development. By focusing our attention on synapses that could be identified at a number of different developmental stages, we found that synaptic connections varied in strength with the age of the specimen. For example, the synaptic connection between a sensory neuron (4x) and the medial giant interneuron (MGI) decreased in strength as the animal matured (Fig. 1A, see legend for methods). We used two measures of synaptic strength: first, the average amplitude of the EPSP (excitatory postsynaptic potential) and second, the probability of detecting an EPSP. The results from 126 synapses recorded in 84 specimens showed that there was a steady decrease in the average EPSP amplitude as the animal matured (Fig. 1B). Three different receptors showed the same trends, although afferents from older hairs, such as 3x (born in the third instar), showed the decrease first followed by successively younger receptors such as 4x and 6x (Fig. 1B). Apparently each newly formed afferent made a strong connection with the MGI, and this synaptic connection then gradually faded away as the animal matured and the hair grew longer. Younger afferents, associated with smaller hairs, were born later in development and took over the function of exciting MGI.